



Universiteit  
Leiden  
The Netherlands

## **MRI Contrast-enhancement with superparamagnetic iron oxide nanoparticles amplify macrophage foam cell apoptosis in human and murine atherosclerosis**

Segers, F.M.E.; Ruder, A.V.; Westra, M.M.; Lammers, T.; Dadfar, S.M.; Roemhild, K.; ... ; Biessen, E.A.L.

### **Citation**

Segers, F. M. E., Ruder, A. V., Westra, M. M., Lammers, T., Dadfar, S. M., Roemhild, K., ... Biessen, E. A. L. (2022). MRI Contrast-enhancement with superparamagnetic iron oxide nanoparticles amplify macrophage foam cell apoptosis in human and murine atherosclerosis. *Cardiovascular Research*. doi:10.1093/cvr/cvac032

Version: Accepted Manuscript  
License: [Creative Commons CC BY-NC 4.0 license](https://creativecommons.org/licenses/by-nc/4.0/)  
Downloaded from: <https://hdl.handle.net/1887/3303464>

**Note:** To cite this publication please use the final published version (if applicable).

1 **MRI Contrast-enhancement with superparamagnetic iron oxide nanoparticles amplify macrophage**  
2 **foam cell apoptosis in human and murine atherosclerosis**

3 Filip M.E. Segers<sup>a,b</sup> PhD, Adele V. Ruder<sup>c</sup>, Marijke M. Westra<sup>a</sup> PhD, Twan Lammers<sup>d</sup> DSc PhD, Seyed  
4 Mohammadali Dadfar<sup>d</sup> PhD, Karolin Roemhild<sup>d,e</sup> MSc, Tin Sing Lam<sup>a</sup> MSc, M. Eline Kooi<sup>f</sup> PhD, Kitty B.J.M.  
5 Cleutjens<sup>c</sup> PhD, Fons K. Verheyen<sup>g</sup> PhD, Geert W.H. Schurink<sup>h</sup> MD PhD, Guido R. Haenen<sup>i</sup> PhD, Theo J.C.  
6 van Berkel<sup>a</sup> PhD, Ilze Bot<sup>a</sup> PhD, Bente Halvorsen<sup>b</sup> PhD, Judith C. Sluimer<sup>c,j\*</sup> PhD, Erik A.L. Biessen<sup>a,c,k\*</sup> PhD

7 **Short title: Iron oxide nanoparticles cause plaque apoptosis**

8 <sup>a</sup> Division of BioTherapeutics, Leiden Academic Centre for Drug Research, Leiden, The Netherlands. <sup>b</sup>  
9 Research Institute of Internal Medicine, University Hospital Oslo, Faculty of Medicine, Oslo, Norway. <sup>c</sup>  
10 Department of Pathology, Cardiovascular Research Institute Maastricht (CARIM), Maastricht University  
11 Medical Center, Maastricht, The Netherlands. <sup>d</sup> Department of Nanomedicine and Theranostics and <sup>e</sup>  
12 Institute of Pathology, RWTH Aachen University, Aachen, Germany. <sup>f</sup> Departments of Radiology and  
13 Nuclear Medicine, <sup>g</sup> Molecular Cell Biology and Electron Microscopy (CRISP), <sup>h</sup> Surgery and <sup>i</sup> Toxicology,  
14 Cardiovascular Research Institute Maastricht (CARIM), Maastricht University Medical Center, Maastricht,  
15 The Netherlands. <sup>j</sup> Cardiovascular Sciences, Edinburgh University, Edinburgh, UK. <sup>k</sup> Institute for  
16 Molecular Cardiovascular Research, RWTH Aachen University, Aachen, Germany.

17 \* Equal contribution

18 **Address for correspondence:**

19 Prof. Dr. Judith Sluimer, or Prof. Dr. Erik Biessen  
20 Department of Pathology, Cardiovascular Research Institute Maastricht (CARIM)  
21 Maastricht University Medical Center (MUMC)  
22 P.O. Box 616, 6200 MD Maastricht, The Netherlands  
23 Telephone: +31 (0) 43 3877675; Fax: +31 (0) 43 3874613  
24 Email: [judith.sluimer@maastrichtuniversity.nl](mailto:judith.sluimer@maastrichtuniversity.nl); [erik.biessen@mumc.nl](mailto:erik.biessen@mumc.nl)

1 **ABSTRACT**

2 **Aims** (Ultra) Small superparamagnetic iron oxide nanoparticles, (U)SPIO, are widely used as magnetic  
3 resonance imaging contrast media and assumed to be safe for clinical applications in cardiovascular  
4 disease. As safety tests largely relied on normolipidemic models, not fully representative of the clinical  
5 setting, we investigated the impact of (U)SPIOs on disease-relevant endpoints in hyperlipidemic models  
6 of atherosclerosis.

7 **Methods and results** RAW264.7 foam cells, exposed *in vitro* to Ferumoxide (dextran-coated SPIO),  
8 Ferumoxtran (dextran-coated USPIO), or Ferumoxytol (carboxymethyl dextran-coated USPIO) (all 1 mg  
9 Fe/ml) showed increased apoptosis and ROS accumulation for Ferumoxide and Ferumoxtran, whereas  
10 Ferumoxytol was tolerated well. Pro-apoptotic (TUNEL<sup>+</sup>) and pro-oxidant activity of Ferumoxide (0.3 mg  
11 Fe/kg) and Ferumoxtran (1 mg Fe/kg) were confirmed in plaque, spleen, and liver of hyperlipidemic  
12 ApoE<sup>-/-</sup> (n=9/group) and LDLR<sup>-/-</sup> (n=9-16/group) mice that had received single IV injections compared to  
13 saline-treated controls. Again, Ferumoxytol treatment (1 mg Fe/kg) failed to induce apoptosis or  
14 oxidative stress in these tissues. Concomitant antioxidant treatment (EUK-8/EUK-134) largely prevented  
15 these effects *in vitro* (-68%, P<0.05) and in plaques from LDLR<sup>-/-</sup> mice (-60%, p<0.001, n=8/group).  
16 Repeated Ferumoxtran injections of LDLR<sup>-/-</sup> mice with pre-existing atherosclerosis enhanced plaque  
17 inflammation and apoptosis but did not alter plaque size. Strikingly, carotid artery plaques of  
18 endarterectomy patients who received Ferumoxtran (2.6 mg Fe/kg) before surgery (n=9) also showed 5-  
19 fold increased apoptosis (18.2 versus 3.7% respectively; p=0.004) compared to controls who did not  
20 receive Ferumoxtran. Mechanistically, neither coating nor particle size seemed accountable for the  
21 observed cytotoxicity of Ferumoxide and Ferumoxtran.

1 **Conclusions** Ferumoxide and Ferumoxtran, but not Ferumoxytol, induced apoptosis of lipid-laden  
2 macrophages in human and murine atherosclerosis, potentially impacting disease progression in  
3 patients with advanced atherosclerosis.

4 **Translational Perspective**

5 Past and ongoing clinical trials with iron-based contrast agents in elderly, hyperlipidemic and/or  
6 cardiovascular patients should evaluate tissue apoptosis and monitor future cardiovascular  
7 complications well beyond the imaging timeframe. Safety studies of newly developed iron-based  
8 contrast agents should also be performed in hyperlipidemic settings.

9 **Keywords:** apoptosis, atherosclerosis, leukocyte, oxidative stress, iron oxide nanoparticles

ACCEPTED MANUSCRIPT

## 1 List of abbreviations

ABTS	2,2'-azino-bis(3-ethylbenzothiazoline-6-sulfonic acid) diammonium salt
ApoE <sup>-/-</sup>	Apolipoprotein E knockout
BAX	BCL2 Associated X, Apoptosis Regulator
CKD	Chronic kidney disease
DAB	3,3'-Diaminobenzidine
FDA	U.S. Food and Drug Administration
GTC	Guanidium isothiocyanate
HPRT	Hypoxanthine-guanine phosphoribosyl transferase
hVLDL	Human very-low-density lipoprotein
IL-1 $\beta$	Interleukin-1 $\beta$
IV	Intravenous
LDLR <sup>-/-</sup>	Low-density lipoprotein receptor knockout
MRI	Magnetic resonance imaging
MTT	3-(4,5-dimethylthiazol-2-yl)-2,5-diphenyl-tetrazoliumbromide
NBT-	
BCIP	Nitro-blue tetrazolium chloride with 5-bromo-4-chloro-3'-indolyphosphate p-toluidine salt
NLRP3	Nucleotide-binding oligomerization domain-like receptor family pyrin domain containing 3
PBS	Phosphate buffered saline
ROS	Reactive oxygen species
SPIO	Small superparamagnetic iron oxide nanoparticles
PET-CT	Positron emission tomography-computed tomography
TCA	Trichloroacetic acid
TEAC	Trolox equivalent antioxidant capacity
TUNEL	Terminal deoxynucleotidyl transferase dUTP nick-end labelling
USPIO	Ultrasmall superparamagnetic iron oxide nanoparticles
WTD	Western-type diet
XIAP	X-linked inhibitor of apoptosis protein

## 1 INTRODUCTION

2 Functional imaging is widely employed to detect rupture-prone atherosclerotic plaques in coronary  
3 artery disease and carotid artery disease patients at risk of clinical symptoms <sup>1</sup>. Rupture-prone plaques  
4 are typified by extensive lipid deposition, inflammation, matrix degradation, and cell death. These  
5 factors eventually lead to fibrous cap rupture and subsequent formation of an atherothrombus <sup>2,3</sup>.

6 Several passive and active molecular imaging modalities have been considered to identify high-  
7 risk plaques, including <sup>18</sup>F-fluoro-deoxyglucose-guided positron emission tomography-computed  
8 tomography (PET-CT), marking plaque inflammation and contrast-enhanced magnetic resonance  
9 imaging (MRI), respectively. MRI offers the advantage of superior spatial resolution, especially when  
10 using small (50-150 nm; SPIO) and ultrasmall (15-30 nm; USPIO) superparamagnetic iron oxide  
11 nanoparticles to enhance signal contrast <sup>4-10</sup>. Upon systemic administration, both formulations are  
12 rapidly cleared by the reticuloendothelial system of lung and liver and by renal excretion, while  
13 accumulation in heart and brain is less pronounced, maximising signal to noise <sup>11</sup>. USPIO extravasation  
14 and uptake by macrophages are considerably increased in inflammation <sup>12-14</sup>, and vascular macrophages  
15 in the atherosclerotic plaque, in abdominal aneurysm, and in the infarcted or inflamed heart show avid  
16 accumulation of these particles <sup>4, 5, 15-20</sup>, rendering them useful for cardiovascular disease imaging.

17 Extensive toxicology studies led to the assumption that (U)SPIO are safe for clinical application  
18 <sup>21-23</sup>. However, this notion is merely based on studies in normolipidemic animal and cell culture models.  
19 In the hyperlipidemic setting of atherosclerosis, vascular macrophages will acquire a foam cell  
20 phenotype, with intracellular free cholesterol deposits, and increased production of reactive oxygen  
21 species (ROS) and susceptibility to apoptosis <sup>24, 25</sup>. Moreover, upon uptake USPIO will accumulate in  
22 endo-lysosomes, where their coating will be degraded and the entrapped iron oxide cargo released <sup>26, 27</sup>.  
23 Besides prolonging the imaging signal, <sup>26, 27</sup> this will also foster an oxidative stress response, which may  
24 well be detrimental to macrophage survival. Moreover, monocyte-derived macrophages were reported

1 to enhance inflammatory cytokine secretion upon exposure to iron oxide particles<sup>28</sup>. This suggests that  
2 (U)SPIO toxicity data obtained in normolipidemic, inflammatory macrophages *in vitro* may not be  
3 representative of the clinical situation. This prompted us to study (U)SPIO in macrophage foam cells, and  
4 in murine and human atherosclerosis to elucidate potentially unfavourable effects under clinically  
5 relevant conditions.

## 6 **METHODS**

### 7 Cell culture

8 The RAW264.7 murine macrophage cell line was grown in DMEM, containing 10% foetal bovine serum  
9 (heat-inactivated for 30 min at 56 °C), 2 mmol/L L-glutamine, 100 U/ml penicillin and 100 µg/ml  
10 streptomycin (all from PAA, Cölbe, Germany), at 37 °C in a humidified atmosphere (5% CO<sub>2</sub>).

11 Human VLDL (hVLDL) was isolated from human serum of healthy volunteers by discontinuous density  
12 gradient centrifugation (using KBr; 40,000 rpm for 22 h)<sup>61</sup>. The VLDL fraction was collected and dialyzed  
13 against PBS containing 1 mM EDTA. RAW264.7 cells were incubated with hVLDL (50 µg/ml) for 20 h and  
14 replaced by medium with or without Ferumoxide (100 µg Fe/ml, Guerbet) or two types of ultrasmall iron  
15 oxide nanoparticles (100 µg Fe/ml): Ferumoxtran (Guerbet, France), and Ferumoxytol (RIENSO, Takeda,  
16 EU tradename for Feraheme, AMAG Pharmaceuticals, USA). Cells were pre-treated with EUK-8  
17 antioxidant 2 h prior to Ferumoxtran treatment (25 µM; Merck Chemicals Ltd., Nottingham, UK).  
18 Viability of RAW cells was assessed using MTT assay (3-(4,5-dimethylthiazol-2-yl)-2,5-diphenyl-  
19 tetrazoliumbromide; Sigma). Apoptosis was quantified in ≥ 3 fields per well, 20x magnification after  
20 terminal deoxynucleotidyl transferase dUTP nick-end labelling (TUNEL) (Roche Diagnostics, Basel,  
21 Switzerland), or by flow cytometry of Annexin V-Oregon green (120 ng/ml).

### 22 Iron content

23 Ferumoxtran (100 µg Fe/ml) uptake by RAW264.7 macrophages and foam cells was determined after  
24 incubation for 1 h at 37 °C. Quantitative determination of iron uptake by inductively coupled plasma

1 atomic emission spectroscopy (ICP-AES; Optima 3300 RL, Perkin Elmer, Courtaboeuf, France) was carried  
2 out after mineralization of the pellet with HNO<sub>3</sub> (3 h at 80 °C).

### 3 Animals and Tissue Harvesting

4 All animal work was performed in compliance with the Dutch government and Directive  
5 2010/63/EU guidelines and approved by national and local review boards (AVD1070020185705). Male  
6 low-density lipoprotein receptor knockout (LDLR<sup>-/-</sup>) or Apolipoprotein E knockout (ApoE<sup>-/-</sup>) mice (aged 12  
7 weeks) were obtained from the local animal facility. Animals were housed in the laboratory animal  
8 facility of Leiden University under standard conditions. Food and water were provided *ad libitum* during  
9 the entire experiment. All animals were housed in individually ventilated cages (GM500, Techniplast) in  
10 groups of up to 5 animals per cage, with bedding (corn cob, Technilab-BMI) and cage enrichment. Cages  
11 were changed weekly, reducing handling of the mice to one handling per week during non-intervention  
12 periods.

13 A pilot study was done with ApoE<sup>-/-</sup> mice (n=3/group) that received a single dose of saline, Ferumoxide  
14 (0.3 mg Fe/kg), or Ferumoxtran (1 mg Fe/kg) after 9 weeks on a western-type diet (WTD, 0.25%  
15 cholesterol, 15% cocoa butter, SDS, Sussex, UK). Based on this, a sample size of 8 single mice per group  
16 was calculated by power analysis. No inclusion or exclusion criteria were set. Cages were randomly  
17 located on the racks. LDLR<sup>-/-</sup> (n=9/group) were fed a WTD for 3 weeks, after which they received weekly  
18 intravenous injections of saline or Ferumoxtran and fed a WTD for 5 consecutive weeks. LDLR<sup>-/-</sup>  
19 (n=8/group) fed a WTD for 14 weeks received either saline, Ferumoxtran, antioxidant EUK-134 (10  
20 mg/kg, Cayman Chemicals, Ann Arbor, MI), or Ferumoxtran with EUK-134, whereby EUK-134 was  
21 administered intraperitoneally 1 h prior to the intravenous injection of Ferumoxtran. In a third  
22 experiment, male LDLR<sup>-/-</sup> (n=9/group) fed a WTD for 9 weeks received a single saline, or Ferumoxtran (1  
23 mg Fe/kg) injection. In all experiments, 24 h after the final injection, mice were anaesthetised using a  
24 single dose of pentobarbital (100 mg/kg i.p.), subjected to blood sampling and *in situ* perfusion-fixation



1 through the left cardiac ventricle. Aortic root, liver and spleen were collected for cryosectioning using a  
2 Leica CM 3050S Cryostat (Leica Instruments, Nassloch, Germany).

### 3 Human tissue collection

4 Atherosclerotic carotid arteries (n=18) were obtained at surgery from patients treated with Ferumoxtran  
5 (2.6 mg Fe/kg, single dose, n=9) and historic control patients (n=9) matched for age, sex and plaque type  
6 (Table 1) to analyse apoptosis in plaque sections <sup>4</sup>. Inclusion and exclusion criteria were described  
7 before <sup>4</sup>. Sample size was calculated based on interpatient MRI enhancement. Collection, storage, and  
8 use of tissue and patient data were performed in agreement with institutional ethical guidelines and the  
9 principles outlined in the Declaration of Helsinki, and approved by the Maastricht University Medical  
10 Center Medical Ethical Committee (MEC00-078b) <sup>4</sup>. Subjects gave informed consent prior to the  
11 inclusion and were enrolled consecutively between 2000 and 2002. Samples were processed and  
12 classified based on plaque morphology as described previously <sup>62</sup>.

### 13 Histology and Morphometry

14 Aortic root cryosections (10  $\mu$ m) were stained with Oil Red O (Sigma) and MoMa-2 (1:50; Serotec,  
15 Oxford, UK) to detect lipid deposits and macrophage content, respectively. Secondary antibody goat  
16 anti-rat IgG-AP (1:100; Sigma, St-Louis, MO, USA) and enzyme substrate nitro-blue tetrazolium chloride  
17 with 5-bromo-4-chloro-3'-indolyphosphate p-toluidine salt (NBT-BCIP, DAKO, Glostrup, Denmark) were  
18 used for MoMa-2 visualization. The primary outcome of apoptotic cells in liver, spleen and  
19 atherosclerotic plaque was detected using TUNEL (Roche Diagnostics, Basel, Switzerland) and visualized  
20 using Nova-Red (DAKO) for mouse and AEC (Sigma) for human sections. Human atherosclerotic plaques  
21 were stained with 8OH-dG (Japan Institute for the Control of Aging, clone N45.1), TUNEL and cleaved  
22 caspase for apoptosis, CD68 to detect ROS, apoptosis, and macrophages, respectively. Quantitative  
23 morphometric analysis of Oil Red O, MoMa-2 and TUNEL was performed using Leica Qwin image  
24 analysis software and a Leica-DM-RE microscope (Leica Imaging Systems, Cambridge, UK). Cells were

1 marked as apoptotic when double positive for TUNEL and DAPI. High-sensitive Perl's iron staining was  
2 performed to visualize iron nanoparticles. Following quenching of endogenous peroxidases by hydrogen  
3 peroxide (0.3% in methanol), slides were incubated for 90 min in 1:1 solution of 2% HCl + 2% potassium  
4 hexacyanoferrate  $\text{Fe}^{2+}$ . After washing, slides were incubated for 20 minutes in 3,3'-  
5 diaminobenzidine (DAB, DAKO). Slides were counterstained with nuclear fast red. Negative control  
6 sections incubated with DAB only were negative. Outcome and data analysis were done blindly.

#### 7 Electron Microscopy

8 Tissue fragments of carotid endarterectomy specimens of  $\sim 1 \text{ mm}^3$  were fixed overnight in 2.5%  
9 glutaraldehyde (Ted Pella, Redding, CA), post-fixed in 1% osmium tetroxide solution, dehydrated and  
10 embedded in epoxy resin. Semi-thin (1  $\mu\text{m}$ ) serial sections were stained with toluidine blue to localize  
11 microvessels. Ultra-thin sections (70-90 nm) were mounted on Formvar (1595 E, Merck)-coated 75 mesh  
12 copper grids, and counterstained with uranyl acetate and lead citrate before analysis on a Philips CM100  
13 transmission electron microscope.

#### 14 Trolox equivalent antioxidant capacity

15 The trolox equivalent antioxidant capacity (TEAC) gives the concentration of 2,2'-azino-bis (3-  
16 ethylbenzthiazoline-6-sulfonic acid) diammonium salt (ABTS) radicals that can be scavenged by serum. It  
17 is a measure of antioxidant capacity. The TEAC was determined in serum that was deproteinated with a  
18 final concentration of 5% trichloroacetic acid (TCA) as described <sup>63</sup>. The samples were incubated with an  
19 ABTS radical solution for 5 min and subsequently, the reduction in absorbance at 734 nm, reflecting the  
20 extent of radical scavenging, was quantified. This is related to that of the reference antioxidant trolox  
21 and is expressed as  $\mu\text{M}$  trolox equivalents. The TEAC value gives the concentration of trolox that has the  
22 same capacity.

#### 23 Uric Acid

1 Uric acid was determined in serum that was deproteinated with a final concentration of 5% TCA, using  
2 HPLC. A Hypersil BDS C-18 end-capped column, 125 x 4 mm, particle size 5  $\mu\text{m}$  (Agilent, Palo Alto, CA,  
3 USA), was used, with a mobile phase of 0.1% trifluoroacetic acid (v/v) in water. UV detection was  
4 performed at 292 nm.

#### 5 IL1- $\beta$ ELISA

6 IL1- $\beta$ , secreted in supernatant medium of RAW cells, was measured as suggested by the manufacturer  
7 (Invitrogen, Breda, The Netherlands).

#### 8 Quantitative RT-PCR

9 Quantitative RT-PCR analysis was performed to determine mRNA expression of apoptosis and oxidative  
10 stress related genes in RAW cells, foam cells and Ferumoxtran-treated foam cells. Total RNA extracts  
11 isolated using the guanidium isothiocyanate (GTC) method<sup>64</sup> were transformed into cDNA using  
12 RevertAid M-MuLV reverse transcriptase (Fermentas, Burlington, Canada) according to manufacturer's  
13 protocol. Quantitative gene expression analysis was performed with the SYBR-Green technology on a  
14 7500 fast Real-Time PCR apparatus (Applied Biosystems, Foster City, CA). All Ct values were normalized  
15 to the stable-expressed reference gene hypoxanthine phospho-ribosyltransferase (HPRT).  
16 Supplementary table 1 shows a detailed overview of the different primer pairs (Eurogentec, Maastricht,  
17 The Netherlands), which were designed using NCBI primer blast.

#### 18 Serum Cholesterol Analysis

19 Total cholesterol concentration in serum was determined using an enzymatic colorimetric assay (Roche  
20 Diagnostics). Precipath I (Roche Diagnostics) was used as an internal standard. Absorbance was  
21 measured at 490 nm. Cholesterol distribution over the different lipoprotein fractions was determined by  
22 fractionation of 30  $\mu\text{l}$  serum using a Superose 6 column (3.2x300mm, Smart-system, Pharmacia,  
23 Uppsala, Sweden). Cholesterol content of the effluent was determined as described above.

#### 24 Dextran uptake assay

1 RAW264.7 cells were seeded at 75 00 cells per well in a 96-well black clear-bottom imaging microplate  
2 (Corning #353219) in DMEM medium with 4.5 g/L D-glucose and pyruvate (Gibco #31966-021)  
3 supplemented with 10% heat-inactivated (30 min at 56 °C) foetal bovine serum (SERANA S-FBS-SA-015)  
4 and 1% penicillin-streptomycin, and left to attach for 2 h (37 °C, 5% CO<sub>2</sub>). Supernatant of cells was either  
5 replaced with 1, 2.4, or 4 μM TRITC-labelled dextran (ThermoFisher Scientific #D7139). After 1 h (37 °C,  
6 5% CO<sub>2</sub>), cells were washed with DMEM and nuclei were stained with Hoechst 33342 (Sigma #B2261) in  
7 DMEM for 10 min (37 °C, 5% CO<sub>2</sub>). Cells were imaged using the BD Pathway 855 (BD Biosciences) and  
8 analysed with CellProfiler software 4.0.4<sup>65</sup>.

9 Chemicals for synthesis of iron particles

10 Ferric chloride anhydrous, ferrous chloride tetrahydrate, 1,10-phenanthroline, hydroxylamine  
11 hydrochloride, dextran and carboxymethyl (CM) dextran were purchased from Sigma-Aldrich (Munich,  
12 Germany). Trisodium citrate dihydrate, citric acid, hydrogen chloride, ammonium hydroxide (NH<sub>4</sub>OH)  
13 and sodium hydroxide were obtained from Carl Roth (Karlsruhe, Germany).

14 Synthesis of citrate-coated iron particles

15 Citrate-coated iron particles were prepared via the standard co-precipitation technique. Briefly, 8 mmol  
16 of ferric chloride was dissolved in 10 ml of deionized water (from here on water) and mixed for 5 min  
17 under mechanical stirring and nitrogen atmosphere. Subsequently, 4 mmol of ferrous chloride  
18 tetrahydrate was added to the solution and mixed for a further 5 min at room temperature. The pH of  
19 the solution was adjusted to 11.0 by adding 80 ml of 1 M aqueous ammonia solution drop-wisely and  
20 vigorously stirred at room temperature for 30 min. The formed black-coloured iron oxide nanoparticles  
21 were decanted using a permanent magnet and washed at least three times with 500 ml of water.  
22 Afterwards, 20 ml of 0.1 M hydrochloric acid was added to the particles and sonicated for 10 min.  
23 Following, 2.5 g trisodium citrate dihydrate in 10 ml of water were added to the mixture and was stirred  
24 at 80 °C for 2 h. The citrate-coated polydisperse particles were separated using a permanent magnet

1 and then resuspended in 35 ml of water. Finally, the suspension was passed through a 0.2  $\mu\text{m}$  filter to  
2 remove larger particles.

3 This highly polydisperse crude batch was subjected to five sequential rounds of centrifugation to obtain  
4 monodispersed iron particle subfractions. As depicted in Supplementary Fig. 1, the supernatant  
5 obtained after 20 min of centrifugation at 14,000 rpm is referred to as Citrate S (USPIO size). The  
6 precipitate was resuspended in water and centrifuged again at progressively lower speed. The  
7 monodisperse batch obtained after 5 centrifugation cycles is referred to as Citrate L (SPIO size).

#### 8 Synthesis of dextran coated iron particles

9 Dextran-coated iron particles were prepared via the standard co-precipitation technique, under a  
10 nitrogen atmosphere. Briefly, 1 mmol of ferric chloride was dissolved in 2 ml of water and mixed for 5  
11 min under mechanical stirring and nitrogen atmosphere. Subsequently, 0.5 mmol of ferrous chloride  
12 tetrahydrate in 1 ml of water was added to the solution and mixed for 5 min at room temperature after  
13 which pH was adjusted to 11.0 (1 M aqueous ammonia). The suspension was stirred at 0 °C for 1 or 30  
14 min to obtain differently sized particles and an aqueous solution of dextran (1 kDa or 10 kDa; 1 gr) or  
15 CM-dextran (10-20 kDa, 1 gr), filtered over a 200 nm syringe filter, was added. The temperature was  
16 slowly increased to 80 °C and was kept at that temperature for 60 min. Afterwards, the solution was  
17 cooled down to room temperature. The formed black-coloured iron oxide particles were sonicated for  
18 20 min. Following, the solution was dialyzed for 24 h against 5 l of water (25 kDa cutoff, SnakeSkin™  
19 dialysis membrane, ThermoFisher Scientific, Massachusetts, USA). Finally, the suspension was passed  
20 through a 0.2  $\mu\text{m}$  filter to remove the aggregates. Also here, the highly polydisperse starting batch was  
21 fractionated by size via two sequential rounds of centrifugation as described above (14,000 rpm, 20 min  
22 (S batch) and 7,000 rpm, 10 min (L batch)).

#### 23 Characterisation of synthesized iron particles

1 Particle size and size distribution, Zeta potential, average hydrodynamic diameter (Dh) and  
2 polydispersity index (PDI) of the particles were measured by dynamic light scattering using a Zetasizer  
3 Nano-ZS instrument (Malvern Instruments, Malvern, UK) at 25 °C. The machine was equipped with a 633  
4 nm He–Ne laser and a detector at angle of 173°. The samples were diluted and sonicated in a water bath  
5 prior to size analysis. Iron concentration was measured using 1,10-phenanthroline assay as described  
6 previously<sup>59</sup>. Finally, the absorbance was detected at 510 nm using an Infinite M200 Pro TECAN reader  
7 (TECAN, Germany).

#### 8 Apoptosis assay

9 RAW264.7 cells were seeded at 6000 cells per well in a 96-well black clear-bottom imaging microplate  
10 (Corning #353219) in DMEM medium with 4.5 g/L D-glucose and pyruvate (Gibco #31966-021)  
11 supplemented with 10% heat-inactivated (30 min at 56 °C) foetal bovine serum (SERANA S-FBS-SA-015)  
12 and 1% penicillin-streptomycin, and left to attach for 24 h (37 °C, 5% CO<sub>2</sub>). Supernatant of cells was  
13 either replaced with 50 µg/ml hVLDL in DMEM or fresh DMEM. After 20 h (37 °C, 5% CO<sub>2</sub>), cells were  
14 incubated with iron particles (100 µg Fe/ml) small (S) or large (L) in size with different coatings (citrate,  
15 dextran, or carboxymethylated dextran) in DMEM or fresh DMEM for 1 h (37 °C, 5% CO<sub>2</sub>). Nuclei were  
16 stained with Hoechst 33342 (Sigma #B2261) in DMEM for 10 min (37 °C, 5% CO<sub>2</sub>). After washing with  
17 Annexin binding buffer (10 mM HEPES, 140 mM NaCl, 5 mM CaCl<sub>2</sub>; pH 7.37), cells were incubated with  
18 2.5 ng/µl Annexin V for 15 min (37 °C, 5% CO<sub>2</sub>). Cells were imaged using the BD Pathway 855 (BD  
19 Biosciences) and analysed with CellProfiler software 4.0.4<sup>66</sup>.

#### 20 Statistical Analysis

21 Data are expressed as mean ± SEM. Normal distribution was assessed by Shapiro-Wilkes normality test,  
22 followed by Student's t-test or ANOVA for normal distributed data or a non-parametric Mann-Whitney U  
23 test or Kruskal-Wallis to compare two or more groups. Sidak or Dunn's multiple comparison test

1 followed significant changes demonstrated by ANOVA or Kruskal-Wallis respectively. Results were  
2 considered statistically different when  $p < 0.05$ .

### 3 **RESULTS**

#### 4 **Iron oxide nanoparticles induce macrophage foam cell apoptosis *in vitro*, plaque, liver and spleen *in*** 5 ***vivo***

6 RAW264.7 foam cells were formed by preloading with 50  $\mu\text{g/ml}$  human very-low-density lipoprotein  
7 (hVLDL) for 20 h. Ninety-minute treatment with the dextran-coated USPIO Ferumoxtran (100  $\mu\text{g Fe/ml}$ )  
8 increased apoptosis of foam cells compared to normolipidemic RAW macrophages (Fig. 1a) in a time-  
9 and hVLDL concentration-dependent manner (Fig. 1e). Specifically, foam cells showed apoptotic  
10 morphology (blebbing and shrinkage) and 4-fold enhanced TUNEL positivity (Fig. 1a-c), despite similar  
11 iron uptake as normolipidemic macrophages (Fig. 1d). Together, these data indicate that Ferumoxtran  
12 preferentially induced apoptosis in lipid-laden foam cells.

13 These findings were confirmed *in vivo* in ApoE<sup>-/-</sup> mice fed a western-type diet (WTD) for 9 weeks  
14 before receiving a single dose of the SPIO platform Ferumoxide (0.3 mg Fe/kg), of Ferumoxtran (1 mg  
15 Fe/kg), or saline. Even these subclinical doses of Ferumoxide or Ferumoxtran markedly enhanced  
16 TUNEL-positive apoptosis in atherosclerotic plaque compared to saline controls (Fig. 2a-d). As expected  
17 from the short follow-up time, plaque size was not affected 24 h after treatment (Fig. 2e), also excluding  
18 that observed effects were biased by differences in plaque stage.

#### 19 **Superparamagnetic iron oxide nanoparticles induce apoptosis in murine liver and spleen *in vivo***

20 Notably, apoptosis was not only limited to atherosclerotic plaques, as macrophage-rich liver and spleen  
21 of ApoE<sup>-/-</sup> mice also showed significant 2.5- to 4-fold increases in TUNEL-positive cells after only a single  
22 dose of Ferumoxide or Ferumoxtran treatment (Fig. 2f, g). TUNEL-positive cells in spleen were  
23 exclusively localised in the red pulp area (Supplementary Fig. 2), which harbours mainly marginal

1 metallophilic macrophages. These data clearly show that Ferumoxide and Ferumoxtran treatment both  
2 enhance apoptosis in atherosclerotic lesions and other macrophage-rich tissue in hyperlipidemic mice.

### 3 **Repeated iron oxide injection show smaller, but less stable plaques**

4 The effect of Ferumoxtran on atherosclerotic lesion progression was studied in LDLR<sup>-/-</sup> mice, fed a WTD  
5 for 3 weeks to develop initial lesions and then subjected to weekly Ferumoxtran injections (1 mg Fe/kg)  
6 for another 5 weeks. Ferumoxtran-treated mice again showed a 5.4-fold increase in TUNEL-positive  
7 plaque cells compared to controls (Fig. 2h-j). Most apoptotic cells were foam cells, and few endothelial  
8 and smooth muscle cells, as inferred from cell morphology and location. Repeated Ferumoxtran  
9 treatment prevented weight gain, but increased serum levels of total, VLDL, and LDL cholesterol  
10 (Supplementary Fig. 3). These findings are in agreement with a study showing that selective depletion of  
11 monocytes/macrophages in circulation and peripheral tissue results in increased (V)LDL-derived  
12 cholesterol levels with reduced atherogenesis<sup>29</sup>. Indeed, atherosclerotic plaque size was reduced in  
13 Ferumoxtran-treated mice (Fig. 2k), despite the moderate serum cholesterol increase. This observation  
14 concurs with known effects of enhanced apoptosis on early atherosclerosis<sup>2</sup>. Notwithstanding increased  
15 apoptosis, plaque macrophage content was increased in Ferumoxtran-treated mice (Fig. 2l), possibly  
16 reflective of influx of new phagocytes upon apoptotic eat-me signals.

### 17 **Antioxidant treatment prevents iron oxide nanoparticle-induced apoptosis *in vitro* and *in vivo***

18 As iron oxide metabolism has been suggested to lead to oxidative stress<sup>26, 27</sup>, we investigated whether  
19 this could explain Ferumoxtran-induced apoptosis. Twenty-four hours after Ferumoxtran injection,  
20 serum antioxidant levels were increased as shown by increased uric acid concentration with a  
21 consequential increase in Trolox equivalent antioxidant capacity (TEAC) (Fig. 3a, b), a common response  
22 to oxidative stress exposure<sup>30</sup>. Uric acid is an established oxidative stress marker. Although uric acid was  
23 previously shown to display moderate antioxidant activity, this seems outweighed by its pro-oxidant and  
24 pro-inflammatory effects<sup>31</sup>. In addition, plaque oxidant damage (8OH-dG) showed a trend to increase



1 (data not shown), and quantitative RT-PCR of Ferumoxtran-treated and control foam cells revealed a  
2 strong upregulation of oxidative stress-related p22phox (also known as neutrophil cytochrome b light  
3 chain), and the pro-apoptotic BCL2 Associated X, Apoptosis Regulator (Bax) and X-linked inhibitor of  
4 apoptosis (XIAP) genes (Fig. 3c). Although nanoparticle-induced reactive oxygen species (ROS) have been  
5 shown to activate the NLR Family Pyrin Domain (NLRP3) inflammasome<sup>32</sup>, Ferumoxtran did neither  
6 enhance serum interleukin-1 $\beta$  (IL-1 $\beta$ ), nor mRNA expression of IL-1 $\beta$  and NLRP3 in liver and spleens *in*  
7 *vivo* (data not shown).

8 Importantly, Ferumoxtran-augmented apoptosis could be prevented by EUK-8 and its more  
9 lipophilic O-methyl derivative EUK-134, both antioxidants with superoxide dismutase, catalase, and  
10 oxyradical scavenging properties<sup>33</sup>. Antioxidant treatment resulted in normalisation of Ferumoxtran-  
11 induced apoptosis *in vitro* (Fig. 3d), as well as in LDLR<sup>-/-</sup> mice with advanced atherosclerosis (Fig. 3e-j).

#### 12 **Superparamagnetic iron oxide nanoparticles associated with enhanced human plaque apoptosis**

13 As Ferumoxtran has been widely used as contrast agent for MRI detection of inflammatory human  
14 atherosclerosis<sup>4, 5</sup>, the potential impact of Ferumoxtran treatment on human disease was studied in  
15 carotid endarterectomy samples. Samples were collected from symptomatic patients that had received  
16 Ferumoxtran (2.6 mg Fe/kg I.V., n=9) 2-11 days prior to surgery, and from control patients (n=9),  
17 matched for sex, age and plaque phenotype (Table 1)<sup>4</sup>. All patients were eligible, gave informed  
18 consent, and completed all steps of the protocol, and were thus included in the analysis. Notably, the  
19 dose used in our mouse model experiments was almost 3 times lower than that used for the clinical  
20 study. Electron microscopy detected Ferumoxtran mainly in macrophages and smooth muscle cells (Fig.  
21 4a-c). The percentage of TUNEL-positive apoptotic cells (Fig. 3d-j; 3.7 $\pm$ 1.4 (95% CI of mean: 0.5-6.9)  
22 versus 18.2 $\pm$ 5.3 (95% CI: 5.9-30.5) for the control and Ferumoxtran group, respectively), as well as the  
23 number of apoptotic cells per plaque area (33.4 $\pm$  11.1 (95% CI: 7.9-59.0) versus 191.2  $\pm$ 48.0 (95% CI:  
24 80.5-301.9) for the control and Ferumoxtran group, respectively) was increased 4-fold in atherosclerotic

1 plaque from Ferumoxtran-treated compared to untreated patients. Most apoptotic cells were  
2 macrophage foam cells (Fig. 4k, l). TUNEL-positive cells co-localised with CD68-positive macrophages  
3 (Fig. 4e, h) and activated caspase-3 (Fig. 4f, i). Thus, the use of Ferumoxtran in patients with  
4 cardiovascular disease aggravated plaque apoptosis, and possibly subsequent plaque instability.

#### 5 **New USPIO formulation does not enhance macrophage apoptosis *in vitro* or *in vivo***

6 The newly developed carboxymethyl dextran-coated USPIO Ferumoxytol has recently been approved by  
7 the United States Food and Drug Administration (FDA) to treat anaemia in chronic kidney patients<sup>34</sup>. In  
8 light of the initial controversy regarding acute side-effects at time of injection<sup>35</sup> and its use in clinical  
9 trials of several cardiovascular diseases<sup>9, 15-19, 36</sup>, this new generation USPIO was also tested *in vivo* and  
10 *in vitro*. In contrast to prior USPIO formulations, Ferumoxytol did not enhance apoptosis in plaques or  
11 liver of hypercholesterolemic LDLR<sup>-/-</sup> mice (Fig. 5a-g). In line, Ferumoxytol did not enhance foam cell  
12 apoptosis *in vitro*, despite positive Perl's iron staining (Fig. 5h-j). This supports a favourable safety profile  
13 of Ferumoxytol for cardiovascular imaging, in line with recent safety reports<sup>37</sup>, and in contrast to  
14 Ferumoxtran and Ferumoxide, the use of which may have side effects on atherosclerotic plaque  
15 stability.

#### 16 **Dextran coating and particle size are not associated with enhanced macrophage apoptosis**

17 Since Ferumoxide and Ferumoxtran particles are coated with dextran, while Ferumoxytol particles are  
18 coated with negatively charged carboxymethylated dextran, the effect of iron particle coating on  
19 macrophage apoptosis was investigated. Dextran was avidly taken up by RAW264.7 macrophages (Fig.  
20 6a, b) but, compared to the untreated control, no significant induction of apoptosis in both foam cells  
21 and normolipidemic macrophages was observed (Fig. 6c, d). Moreover, no significant difference in  
22 apoptosis was observed in both normolipidemic and hVLDL-laden RAW264.7 cells incubated with iron  
23 nanoparticles coated with citrate, dextran, or carboxymethylated dextran (Supplementary Fig. 4).  
24 Particle size itself also did not appear to be a major determinant of USPIO-induced apoptosis

1 (Supplementary Fig. 4). Taken together, these findings suggest that neither particle size nor coating  
2 accounts for the difference in apoptosis induction found between Ferumoxtran and Ferumoxytol.

### 3 **DISCUSSION**

4 Collectively, our findings indicate that administration of previous formulations of superparamagnetic  
5 iron oxide nanoparticles enhances apoptosis in murine and human atherosclerosis. Despite the large  
6 body of evidence supporting the safety of superparamagnetic iron oxide nanoparticles<sup>22, 23</sup>, concern is  
7 growing that (U)SPIO uptake may lead to intracellular release of iron ions, generation of oxidative stress,  
8 and DNA damage, and that it will promote thrombogenicity in the heart<sup>26, 38, 39</sup>. Our study shows that  
9 Ferumoxide and Ferumoxtran induce apoptosis and ROS in lipid-laden macrophages and that its effects  
10 can be prevented by antioxidant treatment *in vivo* and *in vitro*, pointing to iron oxide-induced oxidative  
11 stress as causative factor for USPIO-induced apoptosis. In support of this finding, bare USPIO was seen  
12 to induce endothelial cell apoptosis *in vitro*, which was also mediated by USPIO-related ROS, and  
13 reversed by antioxidant treatment<sup>40, 41</sup>. In fact, we observed occasional endothelial apoptosis in  
14 atherosclerotic plaque after treatment with dextran-coated Ferumoxide (SPIO), and to a lesser extent  
15 Ferumoxtran (USPIO). The apparent preference for foam cell apoptosis may be explained by the  
16 increased susceptibility to apoptosis of lipid-laden foam cells subjected to a second stressor<sup>24</sup>.

17 Moreover, repeated Ferumoxtran treatment of mice with early atherosclerosis not only led to  
18 enhanced plaque apoptosis but also increased plaque macrophage accumulation. Interestingly, this did  
19 not translate in progressive plaque growth. Although the jury is still out on this notion, increased  
20 macrophage apoptosis has indeed been suggested to impede plaque progression in early-stage  
21 atherosclerosis as phagocytic clearance of apoptotic cells is fully operative at this stage<sup>29, 42, 43</sup>. In  
22 contrast, in advanced plaques with compromised efferocytosis<sup>44</sup>, accumulating apoptotic cell debris and  
23 secondary necrosis will directly promote plaque progression by expansion of the necrotic core and  
24 inflammation<sup>2, 45</sup>. As Ferumoxtran exacerbated plaque apoptosis in mice and patients with advanced

1 atherosclerosis, this raises concerns regarding potentially deleterious effects on plaque progression and  
2 destabilisation. This is especially true considering the prolonged residence time of USPIO platforms in  
3 tissue. In fact, in porcine heart, USPIO persisted for several months after intracardiac injection of USPIO-  
4 labelled stem cells <sup>46</sup>. However, our CVD cohort, with its limited group size, is not fit to draw any  
5 conclusions on USPIO treatment-associated clinical adverse events.

6         Considering the widespread cardiovascular and non-cardiovascular clinical use of USPIO, our  
7 findings may have broader impact. USPIO-based imaging has been used for the diagnosis of tumour  
8 metastases, autoimmune diseases, rheumatoid arthritis, for targeted stem cell transfer to the infarcted  
9 heart, and for treatment of anaemia in patients with chronic kidney disease (CKD) <sup>23, 46-48</sup>. Although  
10 Ferumoxtran has been discontinued in 2010 <sup>49</sup>, several trials have been started to test the potential of  
11 similar USPIO platforms for diagnosis of prostate cancer <sup>50,51</sup>, head and neck squamous cell carcinoma <sup>52</sup>,  
12 and aortic dissection <sup>53</sup>. Most applications involve elderly patient populations, expected to suffer from  
13 moderate to advanced atherosclerosis. Nevertheless, Ferumoxytol, a new generation USPIO equipped  
14 with a carboxymethyl dextran coating, appears to display a safer profile for cardiovascular disease.  
15 Biodistribution, macrophage uptake route and speed, and intracellular release of USPIO entrapped iron  
16 are dependent on particle and iron core size and composition, coating chemistry and charge and will  
17 define the particle's pro-oxidant and pro-apoptotic activity. Dextran-coated SPIOs Ferumoxide and  
18 Ferumoxtran, while differently sized, both acted pro-apoptotic, suggesting that coating (chemistry) may  
19 be critical (Table 2) <sup>54-56</sup>. However, it has previously been shown that blocking CD206 or CD11b does not  
20 reduce SPIO uptake by macrophages, indicating that interaction of the dextran coating with  
21 carbohydrate receptors does not notably contribute to SPIO uptake <sup>57</sup>. Our data show that dextran  
22 polymers of similar size and molecular concentration as the derived SPIO were completely inert,  
23 suggesting that particle charge or subtle factors in the SPIO production process may be critical. Net  
24 macrophage uptake (and thus gross iron oxide availability) of Ferumoxide was highest, followed by

1 Ferumoxytol and Ferumoxtran<sup>54, 58</sup>, which underpins that particle intrinsic factors are decisive.  
2 Ferumoxytol uptake, while higher than that of Ferumoxtran, did not enhance apoptosis. As Ferumoxytol  
3 and Ferumoxtran differ in coating chemistry and charge (negatively charged carboxymethyl dextran  
4 versus non-ionic dextran<sup>56</sup>), but not in particle size and core composition, this suggests that the former  
5 factors are indeed instrumental in its toxicity. The lack of toxicity of citrate- versus dextran- versus  
6 carboxymethyl dextran-coated USPIO particles<sup>59</sup> of similar size, suggest however that the driving  
7 determinant may be even more subtle, and relate to differences in coating density or heterogeneity.  
8 Nevertheless, our study may reassure recent investigators and their patients on safe use of Ferumoxytol  
9 <sup>9, 16, 17, 23, 36, 37, 58</sup>.

10 In conclusion, iron-based contrast agents, such as Ferumoxide and Ferumoxtran increase  
11 apoptosis in human and murine atherosclerotic plaque, an effect that can be prevented by antioxidants.  
12 Their administration to patients with advanced lesions may result in plaque destabilization. Although  
13 Ferumoxytol appears to have a safe cardiovascular profile, our findings indicate that caution should be  
14 exercised when applying other iron-based contrast agents in patients with clinical atherosclerosis or  
15 other inflammatory disorders that involve lipid-laden macrophages.

#### 16 **Funding sources**

17 This work was supported by the Dutch Heart Foundation (established investigator NHS 2003T201 to  
18 E.A.L.B., senior postdoc 2016T060 to J.C.S.); Guerbet; two VENI fellowships (916.86.04 to I.B.,  
19 016.116.017 to J.C.S.); a VIDI fellowship of the Netherlands Organization of Scientific Research  
20 (0.16.186.364 to J.C.S.); an ERC consolidator grant (864121 to T.L.); the German Research Foundation  
21 (GRK/RTG2375: 331065168 to T.L.); and the Leducq foundation transatlantic network of excellence  
22 “Modulating autophagy to treat CVD” (15CVD04 to J.C.S).

#### 23 **Data availability statement**

24 The data underlying this article are available in the article and in its online supplementary material.

1 **Conflicts of interest**

2 The principal investigator (E.A.L.B.) has received financial support for this work from Guerbet.

3 **Author contributions**

4 F.S., T.vB. and E.B. were responsible for conception and design. All authors were involved in analysis and  
5 interpretation of data. F.S., A.R., I.B., T.vB., B.H., J.S., and E.B. drafted the manuscript, or revised it  
6 critically for important intellectual content. All authors gave final approval of the submitted manuscript  
7 and agree to be accountable for all aspects of the work in ensuring that questions related to the  
8 accuracy or integrity of any part of the work are appropriately investigated and resolved.

9

ACCEPTED MANUSCRIPT

## 1 REFERENCES

- 2 1. Fayad ZA, Fuster V, Fallon JT, Jayasundera T, Worthley SG, Helft G, Aguinaldo JG, Badimon JJ,  
3 Sharma SK. Noninvasive in vivo human coronary artery lumen and wall imaging using black-  
4 blood magnetic resonance imaging. *Circulation* 2000;**102**:506-510.
- 5 2. Moore KJ, Tabas I. Macrophages in the pathogenesis of atherosclerosis. *Cell* 2011;**145**:341-355.
- 6 3. Virmani R, Kolodgie FD, Burke AP, Finn AV, Gold HK, Tulenko TN, Wrenn SP, Narula J.  
7 Atherosclerotic Plaque Progression and Vulnerability to Rupture Angiogenesis as a Source of  
8 Intraplaque Hemorrhage. *Arterioscler Thromb Vasc Biol* 2005;**25**:2054-2061.
- 9 4. Kooi ME, Cappendijk VC, Cleutjens KB, Kessels AG, Kitslaar PJ, Borgers M, Frederik PM, Daemen  
10 MJ, van Engelshoven JM. Accumulation of ultrasmall superparamagnetic particles of iron oxide  
11 in human atherosclerotic plaques can be detected by in vivo magnetic resonance imaging.  
12 *Circulation* 2003;**107**:2453-2458.
- 13 5. Trivedi RA, JM UK-I, Graves MJ, Cross JJ, Horsley J, Goddard MJ, Skepper JN, Quartey G,  
14 Warburton E, Joubert I, Wang L, Kirkpatrick PJ, Brown J, Gillard JH. In vivo detection of  
15 macrophages in human carotid atheroma: temporal dependence of ultrasmall  
16 superparamagnetic particles of iron oxide-enhanced MRI. *Stroke* 2004;**35**:1631-1635.
- 17 6. Ruehm SG, Corot C, Vogt P, Kolb S, Debatin JF. Magnetic resonance imaging of atherosclerotic  
18 plaque with ultrasmall superparamagnetic particles of iron oxide in hyperlipidemic rabbits.  
19 *Circulation* 2001;**103**:415-422.
- 20 7. Briley-Saebo KC, Mani V, Hyafil F, Cornily JC, Fayad ZA. Fractionated Feridex and positive  
21 contrast: in vivo MR imaging of atherosclerosis. *Magnetic resonance in medicine : official journal*  
22 *of the Society of Magnetic Resonance in Medicine / Society of Magnetic Resonance in Medicine*  
23 2008;**59**:721-730.
- 24 8. Zheng KH, Schoormans J, Stiekema LCA, Calcagno C, Cicha I, Alexiou C, Strijkers GJ, Nederveen  
25 AJ, Stroes ESG, Coolen BF. Plaque Permeability Assessed With DCE-MRI Associates With USPIO  
26 Uptake in Patients With Peripheral Artery Disease. *JACC Cardiovasc Imaging* 2019;**12**:2081-2083.
- 27 9. Smits LP, Tiessens F, Zheng KH, Stroes ES, Nederveen AJ, Coolen BF. Evaluation of ultrasmall  
28 superparamagnetic iron-oxide (USPIO) enhanced MRI with Ferumoxytol to quantify arterial wall  
29 inflammation. *Atherosclerosis* 2017;**263**:211-218.
- 30 10. Dadfar SM, Roemhild K, Drude NI, von Stillfried S, Knüchel R, Kiessling F, Lammers T. Iron oxide  
31 nanoparticles: Diagnostic, therapeutic and theranostic applications. *Adv Drug Deliv Rev*  
32 2019;**138**:302-325.
- 33 11. Hanini A, Schmitt A, Kacem K, Chau F, Ammar S, Gavard J. Evaluation of iron oxide nanoparticle  
34 biocompatibility. *Int J Nanomedicine* 2011;**6**:787-794.
- 35 12. von Zur Muhlen C, von Elverfeldt D, Bassler N, Neudorfer I, Steitz B, Petri-Fink A, Hofmann H,  
36 Bode C, Peter K. Superparamagnetic iron oxide binding and uptake as imaged by magnetic  
37 resonance is mediated by the integrin receptor Mac-1 (CD11b/CD18): implications on imaging of  
38 atherosclerotic plaques. *Atherosclerosis* 2007;**193**:102-111.
- 39 13. Olzinski AR, Turner GH, Bernard RE, Karr H, Cornejo CA, Aravindhan K, Hoang B, Ringenberg MA,  
40 Qin P, Goodman KB, Willette RN, Macphee CH, Jucker BM, Sehon CA, Gough PJ. Pharmacological  
41 inhibition of C-C chemokine receptor 2 decreases macrophage infiltration in the aortic root of  
42 the human C-C chemokine receptor 2/apolipoprotein E-/- mouse: magnetic resonance imaging  
43 assessment. *Arteriosclerosis, thrombosis, and vascular biology* 2010;**30**:253-259.
- 44 14. Rogers WJ, Basu P. Factors regulating macrophage endocytosis of nanoparticles: implications for  
45 targeted magnetic resonance plaque imaging. *Atherosclerosis* 2005;**178**:67-73.
- 46 15. Richards JM, Semple SI, MacGillivray TJ, Gray C, Langrish JP, Williams M, Dweck M, Wallace W,  
47 McKillop G, Chalmers RT, Garden OJ, Newby DE. Abdominal aortic aneurysm growth predicted

- 1 by uptake of ultrasmall superparamagnetic particles of iron oxide: a pilot study. *Circ Cardiovasc*  
2 *Imaging* 2011;**4**:274-281.
- 3 16. Stirrat CG, Alam SR, MacGillivray TJ, Gray CD, Dweck MR, Dibb K, Spath N, Payne JR, Prasad SK,  
4 Gardner RS, Mirsadraee S, Henriksen PA, Semple SI, Newby DE. Ferumoxytol-enhanced magnetic  
5 resonance imaging in acute myocarditis. *Heart* 2018;**104**:300-305.
- 6 17. Stirrat CG, Alam SR, MacGillivray TJ, Gray CD, Dweck MR, Raftis J, Jenkins WS, Wallace WA,  
7 Pessotto R, Lim KH, Mirsadraee S, Henriksen PA, Semple SI, Newby DE. Ferumoxytol-enhanced  
8 magnetic resonance imaging assessing inflammation after myocardial infarction. *Heart*  
9 2017;**103**:1528-1535.
- 10 18. Investigators MRS. Aortic Wall Inflammation Predicts Abdominal Aortic Aneurysm Expansion,  
11 Rupture, and Need for Surgical Repair. *Circulation* 2017;**136**:787-797.
- 12 19. Lagan J, Naish JH, Simpson K, Zi M, Cartwright EJ, Foden P, Morris J, Clark D, Birchall L, Caldwell J,  
13 Trafford A, Fortune C, Cullen M, Chaudhuri N, Fildes J, Sarma J, Schelbert EB, Schmitt M, Piper  
14 Hanley K, Miller CA. Substrate for the Myocardial Inflammation-Heart Failure Hypothesis  
15 Identified Using Novel USPIO Methodology. *JACC Cardiovasc Imaging* 2020.
- 16 20. Trivedi RA, U-King-Im J-M, Graves MJ, Cross JJ, Horsley J, Goddard MJ, Skepper JN, Quartey G,  
17 Warburton E, Joubert I, Wang L, Kirkpatrick PJ, Brown J, Gillard JH. In Vivo Detection of  
18 Macrophages in Human Carotid Atheroma. *Stroke* 2004;**35**:1631-1635.
- 19 21. Muller K, Skepper JN, Posfai M, Trivedi R, Howarth S, Corot C, Lancelot E, Thompson PW, Brown  
20 AP, Gillard JH. Effect of ultrasmall superparamagnetic iron oxide nanoparticles (Ferumoxtran-10)  
21 on human monocyte-macrophages in vitro. *Biomaterials* 2007;**28**:1629-1642.
- 22 22. Bourrinet P, Bengel HH, Bonnemain B, Dencausse A, Idee JM, Jacobs PM, Lewis JM. Preclinical  
23 safety and pharmacokinetic profile of Ferumoxtran-10, an ultrasmall superparamagnetic iron  
24 oxide magnetic resonance contrast agent. *Invest Radiol* 2006;**41**:313-324.
- 25 23. Macdougall IC, Strauss WE, McLaughlin J, Li Z, Dellanna F, Hertel J. A randomized comparison of  
26 Ferumoxytol and iron sucrose for treating iron deficiency anemia in patients with CKD. *Clin J Am*  
27 *Soc Nephrol* 2014;**9**:705-712.
- 28 24. Devries-Seimon T, Li Y, Yao PM, Stone E, Wang Y, Davis RJ, Flavell R, Tabas I. Cholesterol-induced  
29 macrophage apoptosis requires ER stress pathways and engagement of the type A scavenger  
30 receptor. *J Cell Biol* 2005;**171**:61-73.
- 31 25. Hung YC, Hong MY, Huang GS. Cholesterol loading augments oxidative stress in macrophages.  
32 *FEBS Lett* 2006;**580**:849-861.
- 33 26. Briley-Saebo K, Bjornerud A, Grant D, Ahlstrom H, Berg T, Kindberg GM. Hepatic cellular  
34 distribution and degradation of iron oxide nanoparticles following single intravenous injection in  
35 rats: implications for magnetic resonance imaging. *Cell and tissue research* 2004;**316**:315-323.
- 36 27. Fayad ZA, Razzouk L, Briley-Saebo KC, Mani V. Iron oxide magnetic resonance imaging for  
37 atherosclerosis therapeutic evaluation: still "rusty?". *Journal of the American College of*  
38 *Cardiology* 2009;**53**:2051-2052.
- 39 28. Guildford AL, Poletti T, Osbourne LH, Di Cerbo A, Gatti AM, Santin M. Nanoparticles of a  
40 different source induce different patterns of activation in key biochemical and cellular  
41 components of the host response. *J R Soc Interface* 2009;**6**:1213-1221.
- 42 29. Stoneman V, Braganza D, Figg N, Mercer J, Lang R, Goddard M, Bennett M. Monocyte/macrophage  
43 suppression in CD11b diphtheria toxin receptor transgenic mice  
44 differentially affects atherogenesis and established plaques. *Circ Res* 2007;**100**:884-893.
- 45 30. Ames BN, Cathcart R, Schwiers E, Hochstein P. Uric acid provides an antioxidant defense in  
46 humans against oxidant- and radical-caused aging and cancer: a hypothesis. *Proc Natl Acad Sci U*  
47 *S A* 1981;**78**:6858-6862.



- 1 31. Esen AM, Akcakoyun M, Esen O, Acar G, Emiroglu Y, Pala S, Kargin R, Karapinar H, Ozcan O,  
2 Barutcu I. Uric acid as a marker of oxidative stress in dilatation of the ascending aorta. *Am J*  
3 *Hypertens* 2011;**24**:149-154.
- 4 32. Zhou R, Yazdi AS, Menu P, Tschopp J. A role for mitochondria in NLRP3 inflammasome  
5 activation. *Nature* 2011;**469**:221-225.
- 6 33. Rong Y, Doctrow SR, Tocco G, Baudry M. EUK-134, a synthetic superoxide dismutase and  
7 catalase mimetic, prevents oxidative stress and attenuates kainate-induced neuropathology.  
8 *Proc Natl Acad Sci U S A* 1999;**96**:9897-9902.
- 9 34. Lu M, Cohen MH, Rieves D, Pazdur R. FDA report: Ferumoxytol for intravenous iron therapy in  
10 adult patients with chronic kidney disease. *Am J Hematol* 2010;**85**:315-319.
- 11 35. FDA. FDA Drug Safety Communication: FDA strengthens warnings and changes prescribing  
12 instructions to decrease the risk of serious allergic reactions with anemia drug Feraheme  
13 (Ferumoxytol). 2016.
- 14 36. Usman A, Patterson AJ, Yuan J, Cluroe A, Patterson I, Graves MJ, Gillard JH, Sadat U.  
15 Ferumoxytol-enhanced three-dimensional magnetic resonance imaging of carotid atheroma- a  
16 feasibility and temporal dependence study. *Sci Rep* 2020;**10**:1808.
- 17 37. Wetmore JB, Weinhandl ED, Zhou J, Gilbertson DT. Relative Incidence of Acute Adverse Events  
18 with Ferumoxytol Compared to Other Intravenous Iron Compounds: A Matched Cohort Study.  
19 *PLoS One* 2017;**12**:e0171098.
- 20 38. Shen Y, Huang Z, Liu X, Qian J, Xu J, Yang X, Sun A, Ge J. Iron-induced myocardial injury: an  
21 alarming side effect of superparamagnetic iron oxide nanoparticles. *J Cell Mol Med*  
22 2015;**19**:2032-2035.
- 23 39. Nemmar A, Beegam S, Yuvaraju P, Yasin J, Tariq S, Attoub S, Ali BH. Ultrasmall  
24 superparamagnetic iron oxide nanoparticles acutely promote thrombosis and cardiac oxidative  
25 stress and DNA damage in mice. *Part Fibre Toxicol* 2016;**13**:22.
- 26 40. Buyukhatipoglu K, Clyne AM. Superparamagnetic iron oxide nanoparticles change endothelial  
27 cell morphology and mechanics via reactive oxygen species formation. *J Biomed Mater Res A*  
28 2011;**96**:186-195.
- 29 41. Zhu MT, Wang B, Wang Y, Yuan L, Wang HJ, Wang M, Ouyang H, Chai ZF, Feng WY, Zhao YL.  
30 Endothelial dysfunction and inflammation induced by iron oxide nanoparticle exposure: Risk  
31 factors for early atherosclerosis. *Toxicol Lett* 2011;**203**:162-171.
- 32 42. Babaev VR, Chew JD, Ding L, Davis S, Breyer MD, Breyer RM, Oates JA, Fazio S, Linton MF.  
33 Macrophage EP4 deficiency increases apoptosis and suppresses early atherosclerosis. *Cell*  
34 *Metab* 2008;**8**:492-501.
- 35 43. Boesten LS, Zadelaar AS, van Nieuwkoop A, Hu L, Teunisse AF, Jochemsen AG, Evers B, van de  
36 Water B, Gijbels MJ, van Vlijmen BJ, Havekes LM, de Winther MP. Macrophage p53 controls  
37 macrophage death in atherosclerotic lesions of Apolipoprotein E deficient mice. *Atherosclerosis*  
38 2009;**207**:399-404.
- 39 44. Schrijvers DM, De Meyer GR, Kockx MM, Herman AG, Martinet W. Phagocytosis of apoptotic  
40 cells by macrophages is impaired in atherosclerosis. *Arterioscler Thromb Vasc Biol* 2005;**25**:1256-  
41 1261.
- 42 45. Thorp E, Li G, Seimon TA, Kuriakose G, Ron D, Tabas I. Reduced apoptosis and plaque necrosis in  
43 advanced atherosclerotic lesions of Apoe<sup>-/-</sup> and Ldlr<sup>-/-</sup> mice lacking CHOP. *Cell metabolism*  
44 2009;**9**:474-481.
- 45 46. Kawamura M, Miyagawa S, Fukushima S, Saito A, Miki K, Ito E, Sougawa N, Kawamura T, Daimon  
46 T, Shimizu T, Okano T, Toda K, Sawa Y. Enhanced survival of transplanted human induced  
47 pluripotent stem cell-derived cardiomyocytes by the combination of cell sheets with the  
48 pedicled omental flap technique in a porcine heart. *Circulation* 2013;**128**:S87-94.

- 1 47. Harisinghani MG, Barentsz J, Hahn PF, Deserno WM, Tabatabaei S, van de Kaa CH, de la Rosette  
2 J, Weissleder R. Noninvasive detection of clinically occult lymph-node metastases in prostate  
3 cancer. *N Engl J Med* 2003;**348**:2491-2499.
- 4 48. Beckmann N, Falk R, Zurbrugg S, Dawson J, Engelhardt P. Macrophage infiltration into the rat  
5 knee detected by MRI in a model of antigen-induced arthritis. *Magn Reson Med* 2003;**49**:1047-  
6 1055.
- 7 49. Bietenbeck M, Florian A, Sechtem U, Yilmaz A. The diagnostic value of iron oxide nanoparticles  
8 for imaging of myocardial inflammation – quo vadis? *Journal of Cardiovascular Magnetic  
9 Resonance* 2015;**17**:54.
- 10 50. Ferumoxtran-10-enhanced MRI in Prostate Cancer Patients.  
11 <https://ClinicalTrials.gov/show/NCT04261777>.
- 12 51. Radio Guided Lymph Node Dissection in Oligometastatic Prostate Cancer Patients.  
13 <https://ClinicalTrials.gov/show/NCT04300673>.
- 14 52. Validation of USPIO-enhanced MRI for Detection of Lymph Node Metastases in Head and Neck  
15 Carcinoma. <https://ClinicalTrials.gov/show/NCT03817307>.
- 16 53. Magnetic Resonance Imaging (MRI) for Aortic Dissection to Visualise Inflammation.  
17 <https://ClinicalTrials.gov/show/NCT03948555>.
- 18 54. Modo MMJJ, Bulte JWM. Molecular and cellular MR imaging. Boca Raton: CRC Press, 2007.
- 19 55. Alam SR, Stirrat C, Richards J, Mirsadraee S, Semple SI, Tse G, Henriksen P, Newby DE. Vascular  
20 and plaque imaging with ultrasmall superparamagnetic particles of iron oxide. *J Cardiovasc  
21 Magn Reson* 2015;**17**:83.
- 22 56. Wang G, Serkova NJ, Groman EV, Scheinman RI, Simberg D. Feraheme (Ferumoxytol) Is  
23 Recognized by Proinflammatory and Anti-inflammatory Macrophages via Scavenger Receptor  
24 Type AI/II. *Mol Pharm* 2019;**16**:4274-4281.
- 25 57. Chao Y, Karmali PP, Simberg D. Role of carbohydrate receptors in the macrophage uptake of  
26 dextran-coated iron oxide nanoparticles. *Adv Exp Med Biol* 2012;**733**:115-123.
- 27 58. Yancy AD, Olzinski AR, Hu TC, Lenhard SC, Aravindhana K, Gruver SM, Jacobs PM, Willette RN,  
28 Jucker BM. Differential uptake of Ferumoxtran-10 and Ferumoxytol, ultrasmall  
29 superparamagnetic iron oxide contrast agents in rabbit: critical determinants of atherosclerotic  
30 plaque labeling. *Journal of magnetic resonance imaging : JMRI* 2005;**21**:432-442.
- 31 59. Dadfar SM, Camozzi D, Darguzyte M, Roemhild K, Varvarà P, Metselaar J, Banala S, Straub M,  
32 Güvener N, Engelmann U, Slabu I, Buhl M, van Leusen J, Kögerler P, Hermanns-Sachweh B,  
33 Schulz V, Kiessling F, Lammers T. Size-isolation of superparamagnetic iron oxide nanoparticles  
34 improves MRI, MPI and hyperthermia performance. *Journal of Nanobiotechnology* 2020;**18**:22.
- 35 60. Said B, McCart JA, Libutti SK, Choyke PL. Ferumoxide-enhanced MRI in patients with colorectal  
36 cancer and rising CEA: surgical correlation in early recurrence. *Magn Reson Imaging*  
37 2000;**18**:305-309.
- 38 61. Redgrave TG, Roberts DC, West CE. Separation of plasma lipoproteins by density-gradient  
39 ultracentrifugation. *Anal Biochem* 1975;**65**:42-49.
- 40 62. Virmani R, Kolodgie FD, Burke AP, Farb A, Schwartz SM. Lessons from sudden coronary death: a  
41 comprehensive morphological classification scheme for atherosclerotic lesions. *Arterioscler  
42 Thromb Vasc Biol* 2000;**20**:1262-1275.
- 43 63. Fischer MA, Gransier TJ, Beckers LM, Bekers O, Bast A, Haenen GR. Determination of the  
44 antioxidant capacity in blood. *Clin Chem Lab Med* 2005;**43**:735-740.
- 45 64. Chomczynski P, Sacchi N. Single-step method of RNA isolation by acid guanidinium thiocyanate-  
46 phenol-chloroform extraction. *Anal Biochem* 1987;**162**:156-159.
- 47 65. Lamprecht MR, Sabatini DM, Carpenter AE. CellProfiler: free, versatile software for automated  
48 biological image analysis. *Biotechniques* 2007;**42**:71-75.

## 1 **FIGURE LEGENDS**

### 2 **Figure 1 Ferumoxtran exposure increased apoptosis of RAW foam cells compared to normolipidemic** 3 **macrophages**

4 (a) RAW264.7 cells were transformed into foam cells (20 h incubation with hVLDL 50  $\mu\text{g/ml}$ ) and  
5 incubated with Ferumoxtran (USPIO, 100  $\mu\text{g Fe/ml}$ ). (b) Fluorescent microscopic pictures of DAPI and  
6 TUNEL-stained foam cells incubated with or without Ferumoxtran for 1.5 h. (c) RAW264.7 control  
7 macrophages (circles) and foam cells (squares) were harvested at different time points and cytopspins  
8 were analysed for TUNEL in 3 random fields of view (magnification 20x;  $412 \pm 104$  cells/cytopsin were  
9 analysed). (d) The ability of macrophages and foam cells to take up iron-based contrast media was  
10 quantitatively analysed using an ICP-AES assay. (e) Cell viability after Ferumoxide (100  $\mu\text{g Fe/ml}$ , black  
11 circles) or Ferumoxtran treatment (white circles) of RAW264.7 cells with different lipid loading were  
12 determined using a cytotoxic MTT assay. Data are mean  $\pm$  SEM (n=3), 4-12 technical replicates, and  
13 representative of three independent experiments. Statistics: unpaired student's t-test, \*  $p < 0.05$ , \*\*  
14  $p < 0.01$  and \*\*\*  $p < 0.001$  compared to control conditions. CON: control.

### 15 **Figure 2 Ferumoxide and Ferumoxtran increased apoptosis in atherosclerotic lesions in hyperlipidemic** 16 **ApoE<sup>-/-</sup> and LDLr<sup>-/-</sup> mice**

17 (a) ApoE<sup>-/-</sup> mice with advanced atherosclerosis were injected once with NaCl 0.9% (n=3), Ferumoxide (0.3  
18 mg Fe/kg; n=3) or Ferumoxtran (1 mg Fe/kg; n=3). TUNEL-positive cells in the atherosclerotic plaques of  
19 the aortic root were quantified and normalised to total cell count. \* indicates p-value  $< 0.05$  for Kruskal-  
20 Wallis across three groups, not significant changes in Dunn's post-hoc testing between individual  
21 groups. (b) Representative image of TUNEL staining of plaques in control, (c) Ferumoxide or (d)  
22 Ferumoxtran-treated mice. Scale bar in (b) to (d) corresponds to 100  $\mu\text{m}$ . (e) Plaque area of ApoE<sup>-/-</sup> was  
23 determined by computer-assisted morphometric analysis of Oil red O-stained section. (f) The percentage  
24 of TUNEL-positive cells was quantified in liver and (g) spleen of ApoE<sup>-/-</sup> mice controls and mice receiving  
25 a single Ferumoxide or Ferumoxtran dose. \* indicates p-value  $< 0.05$  for Kruskal-Wallis across three  
26 groups, # p-value  $< 0.05$  in Dunn's post-hoc testing versus control. (h) LDLR<sup>-/-</sup> mice with initial plaques

1 were fed a high cholesterol diet and received weekly intravenous injections with NaCl 0.9% (control  
2 group, n=8) or Ferumoxtran (n=8). The percentage of TUNEL-positive cells was quantified in the  
3 atherosclerotic plaques of the aortic root. Unpaired student's t-test, \* p<0.05 and \*\*\* p<0.001  
4 compared to control conditions. (i) Representative image of TUNEL staining of plaques in control, and (j)  
5 Ferumoxtran-treated LDLR<sup>-/-</sup> mice. (k) Plaque area (Oil red O) and (l) the percentage of macrophages  
6 (MoMa-2-positive) cells were quantified in plaques of control LDLR<sup>-/-</sup> and mice repeatedly treated with  
7 Ferumoxtran. Statistics: unpaired student's t-test, \* p<0.05 and \*\*\* p<0.001 compared to control  
8 conditions. Data are mean ± SEM. CON: control.

9 **Figure 3 Ferumoxtran triggered ROS-induced apoptosis *in vitro* and *in vivo***

10 (a) Serum uric acid and (b) Trolox equivalent antioxidant capacity were increased in serum samples of  
11 LDLR<sup>-/-</sup> mice 24 h after Ferumoxtran injection compared to control, a common response to oxidant stress  
12 exposure. Statistics: unpaired Student's T-test. Data are mean ± SEM. (c) Gene expression levels of  
13 apoptosis- and oxidative stress-related genes of RAW untreated macrophages (white bars), hVLDL-  
14 treated foam cells (yellow bars), and hVLDL-treated foam cells exposed to 100 µg/ml Ferumoxtran  
15 (yellow dotted bars). (d) RAW264.7 cells transformed into foam cells with hVLDL (yellow bars) were  
16 incubated with Ferumoxtran (dotted filling) to induce apoptosis. Pre-treatment of hVLDL foam cells with  
17 antioxidant (grey bars) prior to Ferumoxtran reduced apoptosis. Untreated RAW264.7 cells were used as  
18 a control (white bars). Cells were harvested, cytopins were made and apoptotic cells quantified by  
19 TUNEL analysis in 4 randomly chosen field of views (20x magnification; average 93 ± 27 cells/fov  
20 analyzed). Data are mean ± SEM, include 3-6 technical replicates, and are representative of three  
21 independent experiments. Statistics: \* p<0.05, and p<0.001 versus control (Kruskal-Wallis; Dunn's  
22 multiple comparison). (e) LDLR<sup>-/-</sup> mice on a high cholesterol diet for 6 weeks received a single treatment  
23 with either saline (n=8), saline with antioxidant EUK-134 (10 mg/kg, n=8), Ferumoxtran alone (1000 µg  
24 Fe/kg, n=9), or Ferumoxtran with EUK-134 (n=9). The percentage of TUNEL-positive cells was quantified

1 in the atherosclerotic plaques of the aortic root. Statistics: \*  $p < 0.05$ , and  $p < 0.001$  versus control  
2 (ANOVA; Sidak's multiple comparison). (f) Plaque area (Oil red O) was quantified in plaques of LDLR<sup>-/-</sup>  
3 treated once with saline, EUK-134, Ferumoxtran, or Ferumoxtran with EUK-134. (g) Representative  
4 image of TUNEL staining of plaques in saline, (h) EUK-134, (i) Ferumoxtran, or (j) Ferumoxtran with EUK-  
5 134 treated LDLR<sup>-/-</sup> mice. Data are mean  $\pm$  SEM. CON: control.

#### 6 **Figure 4 Ferumoxtran increased apoptosis in human carotid atherosclerotic lesions**

7 a) Electron microscopy shows human carotid atherosclerotic plaque with accumulation of  
8 superparamagnetic iron oxide nanoparticles, scale bar corresponds to 10  $\mu\text{m}$ . Boxed region shows  
9 particle-laden macrophages, represented in (b) high power view of macrophage with intracellular  
10 Ferumoxtran (arrows). Scale bar corresponds to 2  $\mu\text{m}$ . (c) Smooth muscle cell with numerous  
11 mitochondria (\*) also showing intracellular accumulation of Ferumoxtran nanoparticles (arrow). Insert  
12 shows origin of smooth muscle cell. Scale bar corresponds to 0.5  $\mu\text{m}$ . (d) Atherosclerotic lesions  
13 obtained from symptomatic patients undergoing carotid endarterectomy and receiving no injection  
14 (n=9, d-f) or a single dose of Ferumoxtran (2.7 mg/kg IV, n=9, g-i) prior to surgery. Sections were stained  
15 with TUNEL (AEC red precipitate, d, g). Apoptotic TUNEL-positive cells co-localise with macrophages and  
16 activated caspase-3 on serial sections stained respectively with CD68 (red precipitate; e, h), (f) activated  
17 caspase 3 (red precipitate; f, i). Scale bars in (d) to (i) corresponds to 100  $\mu\text{m}$ . (j) Apoptosis was  
18 quantified as TUNEL-positive cells per total cell count. (k) Arrows indicate TUNEL-positive nuclei in  
19 endothelial cells lining an intraplaque microvessel and (l) smooth muscle cells. Scale bars in (k) and (l)  
20 correspond to 100  $\mu\text{m}$ . Data are mean  $\pm$  SEM. Statistics: \*\*  $p = 0.004$  (Mann-Whitney compared to  
21 control). CON: control.

#### 22 **Figure 5 Ferumoxytol did not enhance apoptosis *in vivo* or *in vitro***

23 a) Plaque area at sacrifice of LDLR<sup>-/-</sup> mice with early atherosclerosis which were fed a high cholesterol  
24 diet for 9 weeks after single weekly intravenous injections with NaCl 0.9% (control group, n=8) or

1 Ferumoxytol (n=8). Representative images of apoptotic cells detected by TUNEL in atherosclerotic  
2 plaques of the aortic root of LDLr<sup>-/-</sup> mice injected with saline (control, b) or Ferumoxytol (c), with  
3 corresponding quantification (d). Quantification (e) and representative images of apoptotic cells  
4 detected by TUNEL in liver of LDLr<sup>-/-</sup> mice injected with saline (control, f) or Ferumoxytol (g). (h) Perl's  
5 iron staining of RAW cells, incubated with hVLDL and Ferumoxytol, detects iron accumulation. (i) Oil red  
6 O staining of RAW cells, incubated with hVLDL and Ferumoxytol, confirmed massive lipid accumulation.  
7 (j) The percentage of apoptotic, Annexin V-positive cells was quantified by flow cytometry of RAW cells  
8 incubated with or without hVLDL, in the absence or presence of Ferumoxytol (n=5-8 technical replicates  
9 per group). Data are mean ± SEM. \* p<0.05, (unpaired Mann-Whitney test or Kruskal-Wallis with Dunn's  
10 multiple comparison test, compared to control). CON: control.

11 **Figure 6 Dextran does not increase apoptosis in RAW foam cells compared to normolipidemic**  
12 **macrophages**

13 (a) Fluorescent microscopic pictures of RAW264.7 incubated with 1 μM, 2.4 μM or 4 μM TRITC-dextran  
14 for 1 h or untreated RAW264.7 (CON) and stained with Hoechst 33342. Per well, 9 fluorescent images  
15 were taken and merged, corresponding to around 2700 cells imaged per well, with 3 technical replicates  
16 per condition. Scale bars correspond to 50 μm. (b) Quantification of (a), percentage of cells positive for  
17 TRITC-dextran. (c) Fluorescent microscopic pictures of RAW264.7 transformed into foam cells with  
18 hVLDL (yellow bars) or normolipidemic cells (white bars) exposed to 2.4 μM or 4.8 μM dextran or fresh  
19 DMEM for 1 h. Untreated cells served as control (CON), RAW264.7 cells treated with 1 μM staurosporine  
20 for 20 h served as positive control (POS). Cells were stained with Annexin V and Hoechst 33342. 9  
21 fluorescent images were taken and merged per well, corresponding to around 4400 cells imaged per  
22 well, with 3 (POS) or 7-8 technical replicates per conditions. Scale bars correspond to 100 μm. (d)  
23 Quantification of (c), percentage of cells positive for Annexin V. Data are presented as mean ± SEM and  
24 representative of three independent experiments (c, d). Statistics: \* p<0.05 (Kruskal-Wallis with Dunn's  
25 multiple comparison test).

26

1 **Table 1 Patient characteristics**

Patient characteristics	Control (n=9)	Ferumoxtran (n=9)
Gender % male; male/female	89%; 8/1	89%; 8/1
Age years+/- SD	64.6±2.9	63.9±3.2
Plaque type thin/thick cap fibroatheroma	67% (n=6)	67% (n=6)
intraplaque/luminal thrombus	33% (n=3)	33% (n=3)
Clinical stage % symptomatic	100%	100%
Stenosis percentage patients with >70%	100%	100%

2 No significant p-values.

3

4 **Table 2 Nanoparticle characteristics**

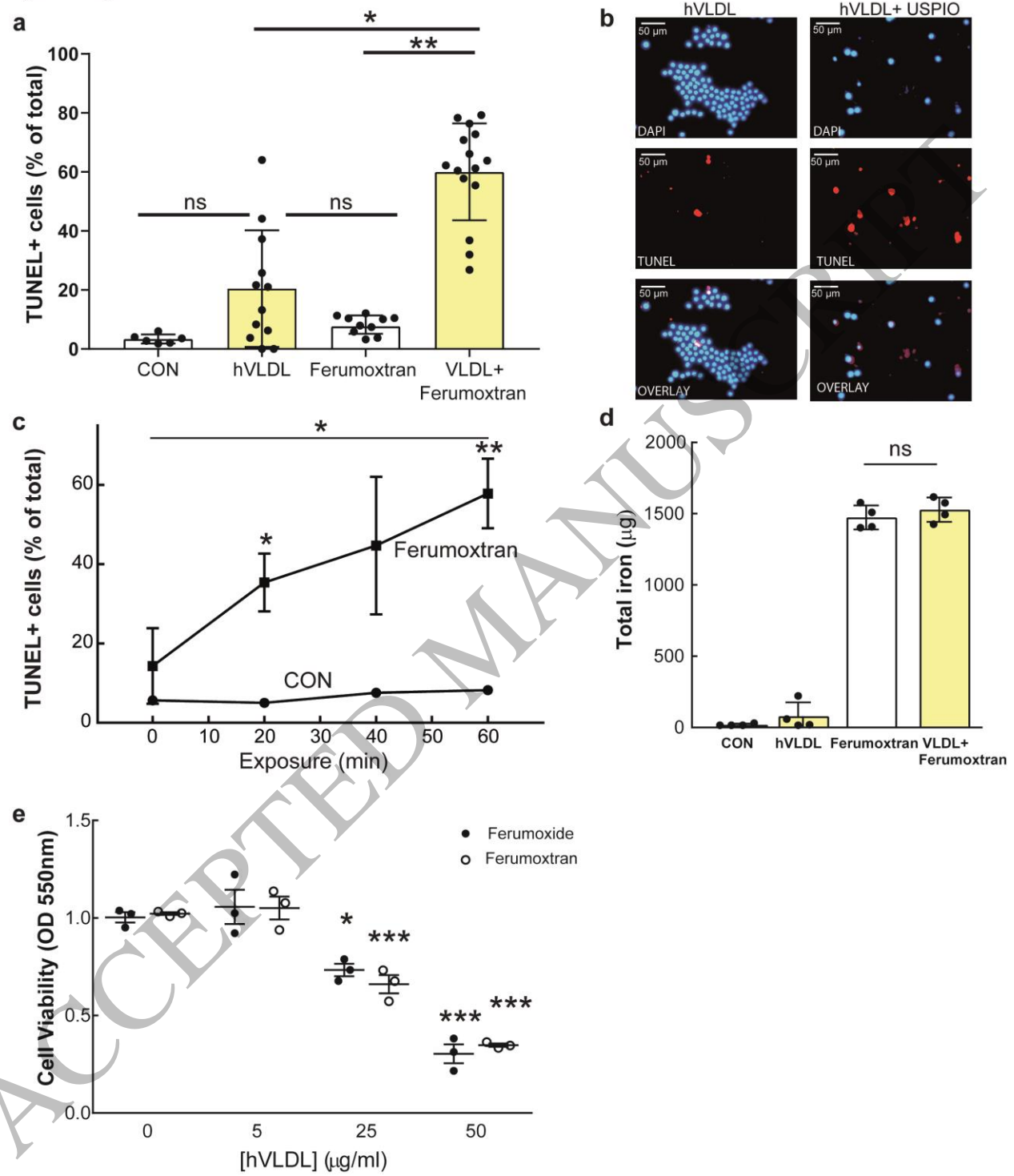
Feature	Ferumoxide	Ferumoxtran	Ferumoxytol
SPIO/USPIO	SPIO	USPIO	USPIO
Particle size (nm)	120-180	31±5	28±4
Crystal core size (nm)	5	6	6.7
Polydispersity index	n.a.	0.374±0.019	0.252±0.018
Half-life (h)	2-3	30	15
Coating	Dextran	Dextran	Carboxymethyl dextran
Zeta potential ζ (mV)	n.a.	-27±7.1	-43.9±8.4
Macrophage uptake (pg Fe/cell)*	5.0-7.0	0.5-1.8	1.0-1.5
Mechanism uptake	SRA1	SRA1	SRA1
Clinical dose mg/kg	0.6	4	2.7

5 Integrated data from <sup>54-56, 60</sup> and own measurements; \*THP-1 with 200 µg Fe/ml for 24 h; SRA1:

6 scavenger-receptor A mediated; n.a.: information not available

7

Figure 1 Segers et al



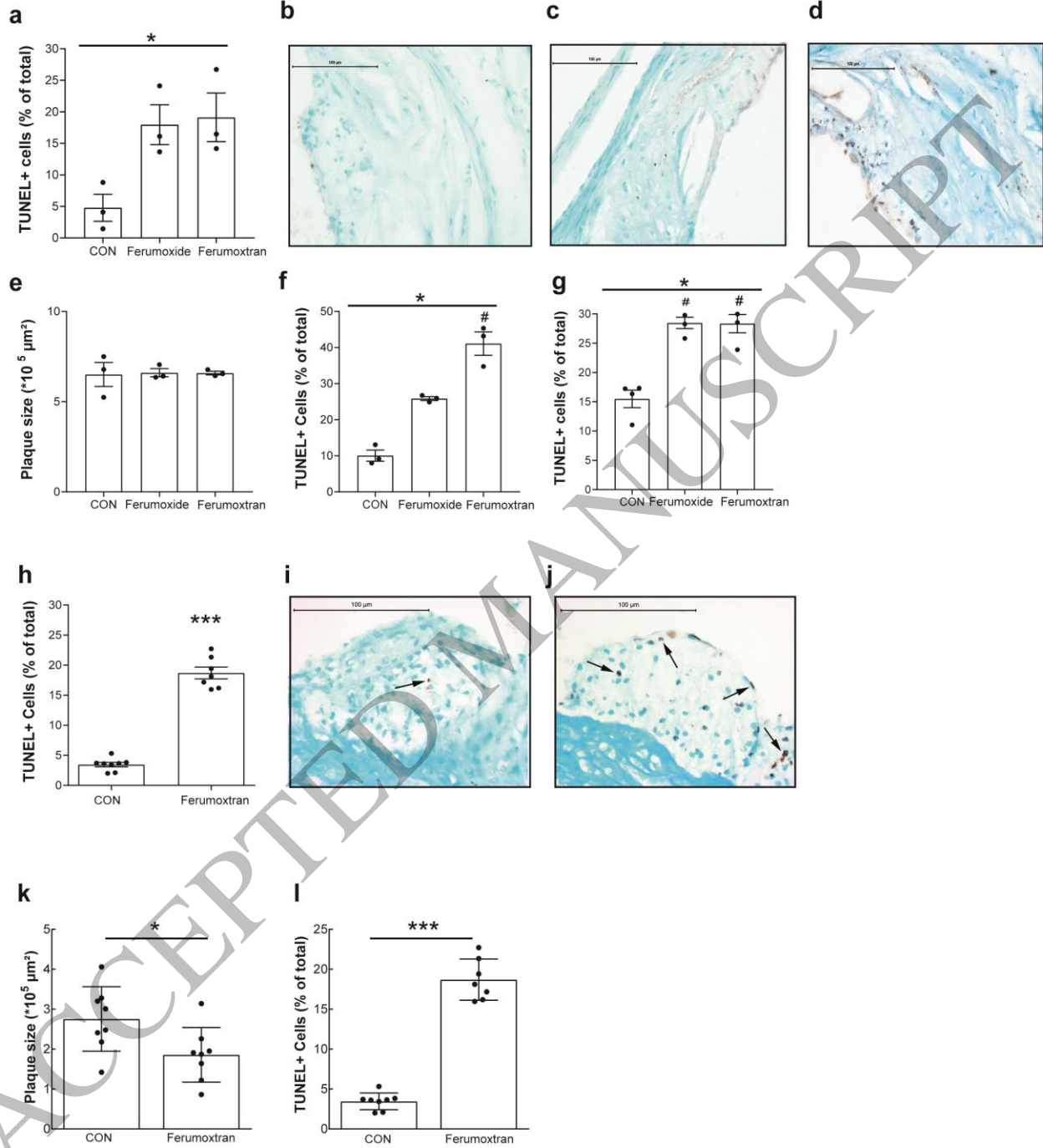
Downloaded from https://academic.oup.com/cv/advance-article/doi/10.1093/cvr/cvab032/6553202 by guest on 13 April 2022

1  
2  
3

165x198 mm (8.9 x DPI)



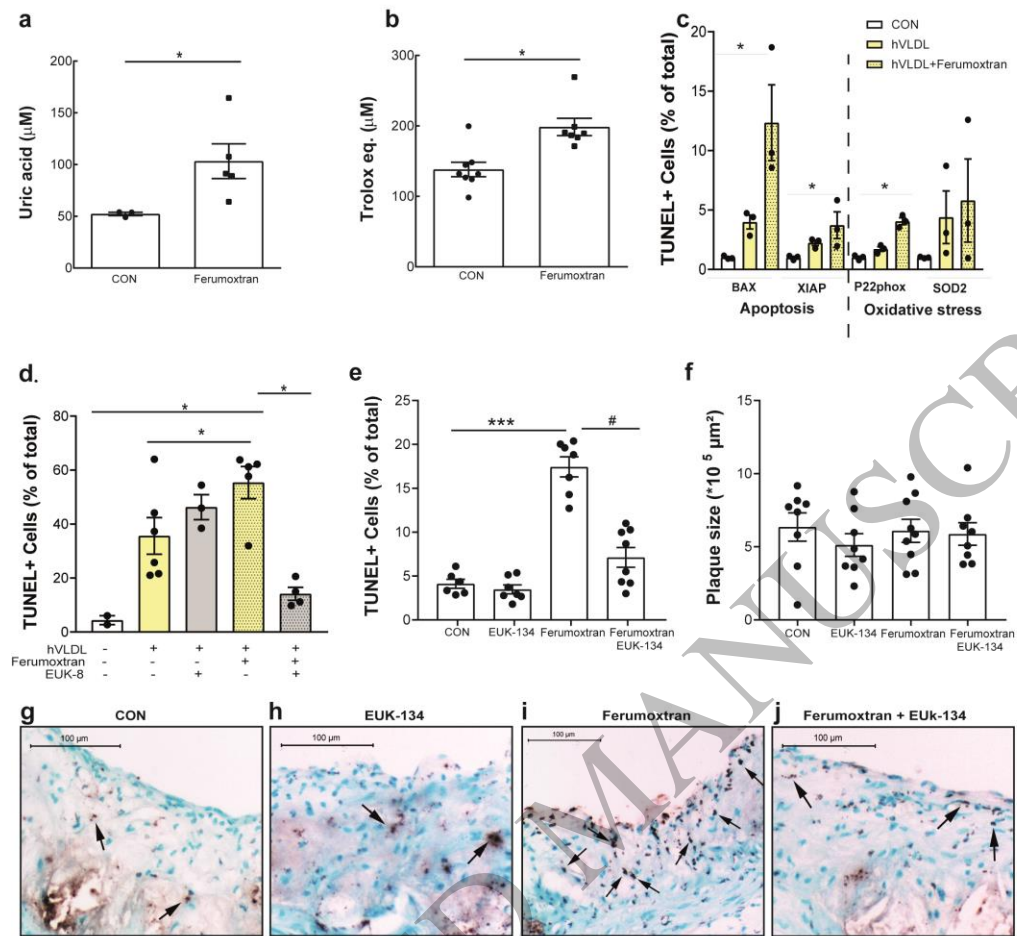
Figure 2 Segers et al



165x191 mm (8.9 x DPI)

1  
2  
3

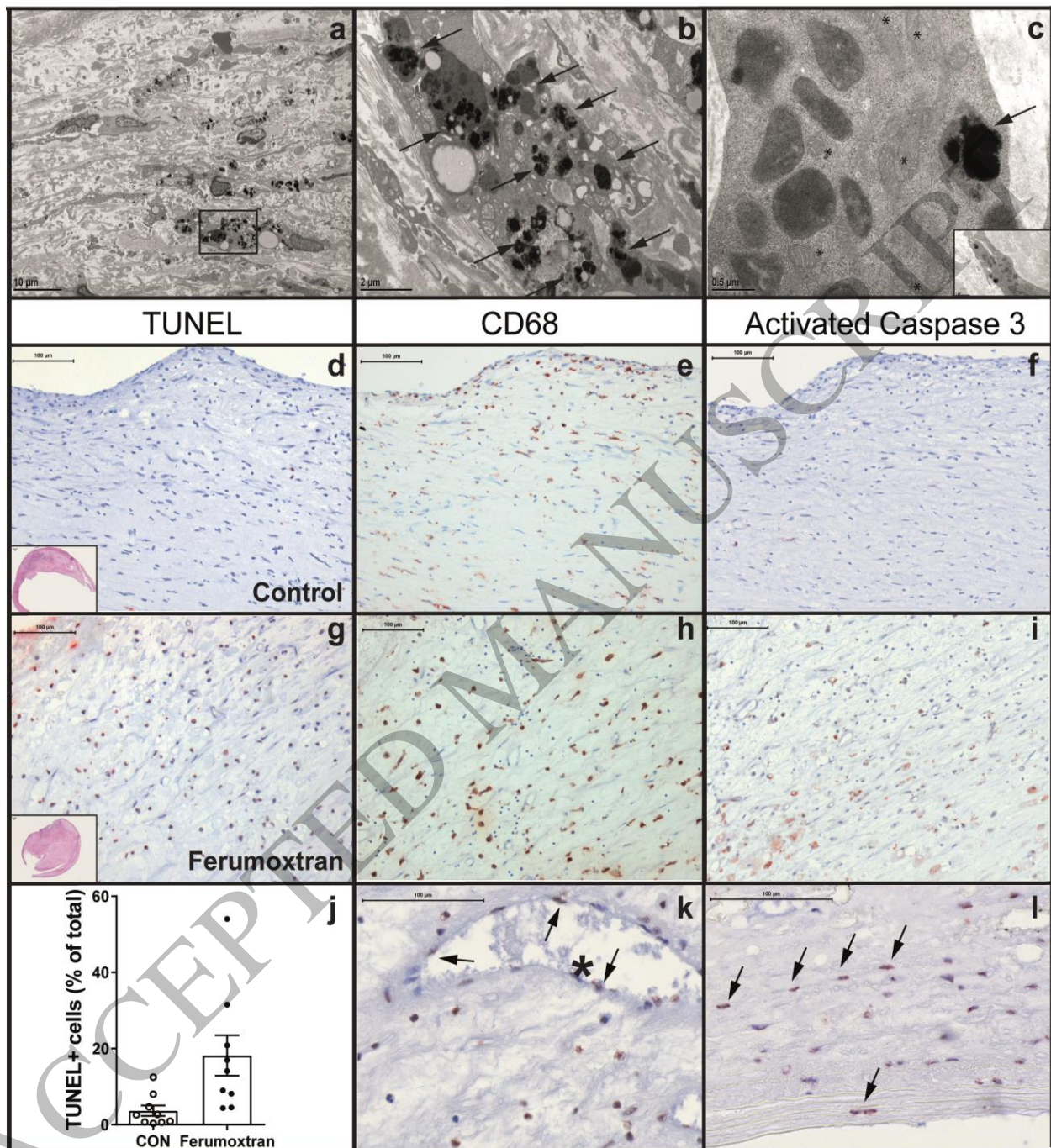
Figure 3 Segers et al



1  
2  
3  
4

165x135 mm (8.9 x DPI)

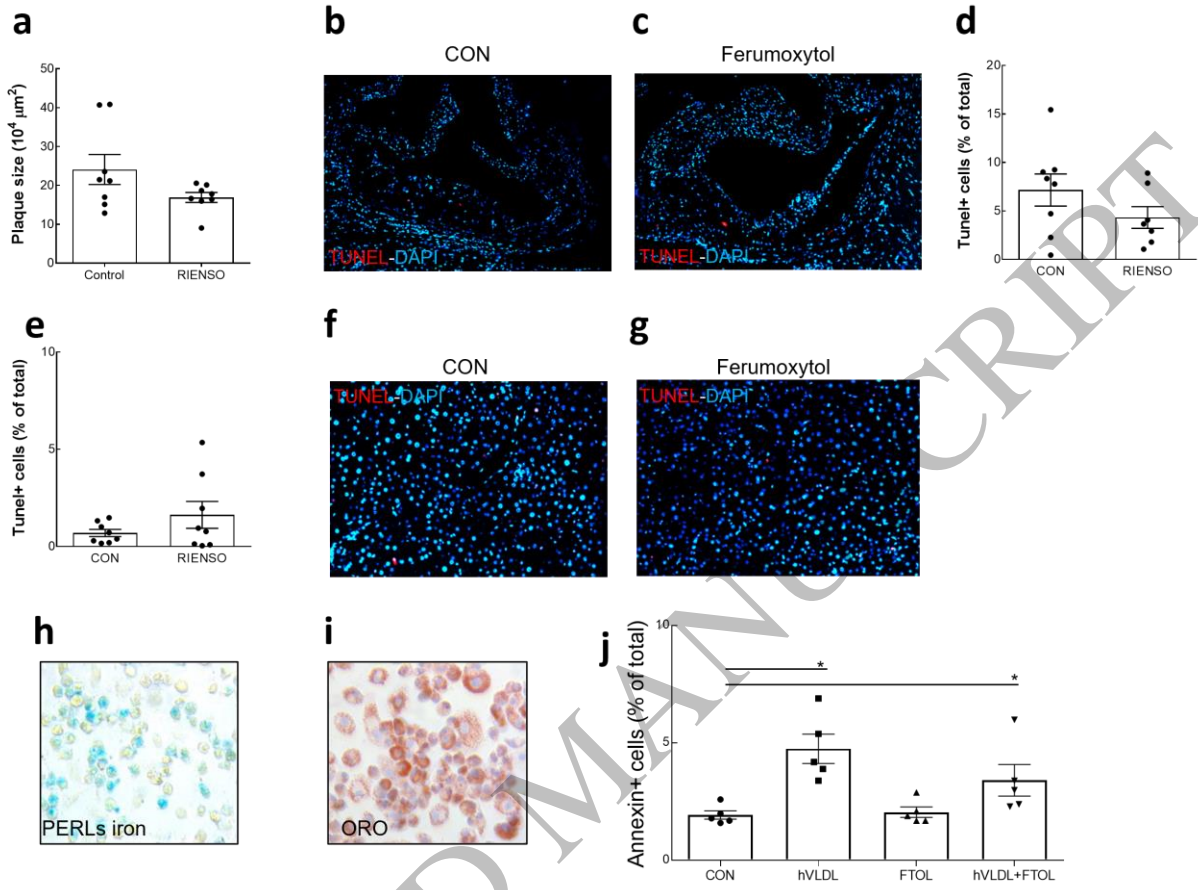
Figure 4 Segers et al



165x185 mm (8.9 x DPI)

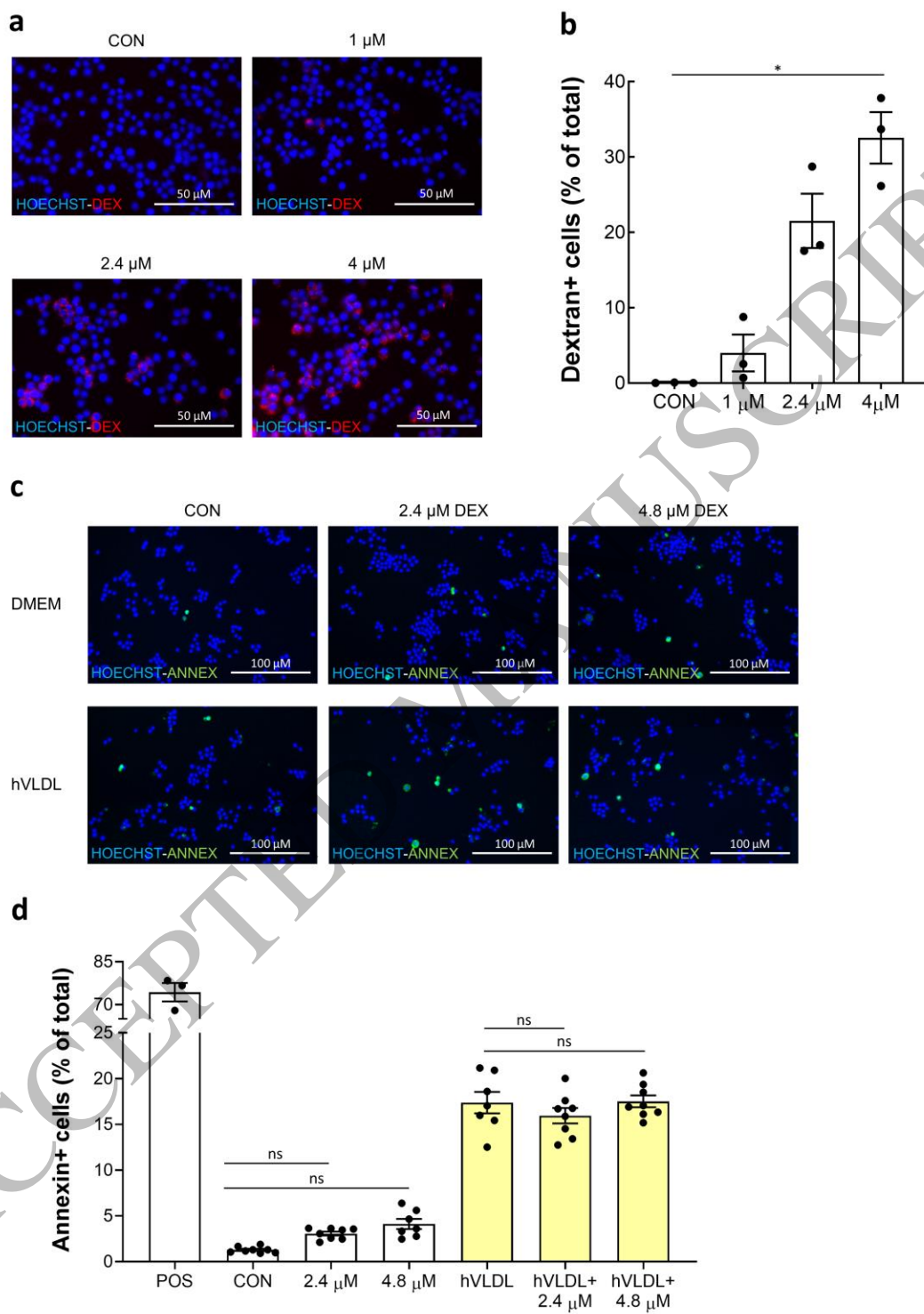
1  
2  
3  
4

Figure 5 Segers et al



165x126 mm (8.9 x DPI)

1  
2  
3



1  
2

158x229 mm (8.9 x DPI)